Quantifying Proton Density in Cortical Bone In-Vivo by 3D Ultra-short Echo-time Imaging

H. Saligheh Rad[1], S. Lam[1], J. Love[1], J. F. Magland[1], and F. W. Wehrli[1]
[1]Laboratory for Structural NMR Imaging, Department of Radiology, University of Pennsylvania Health System, Philadelphia, PA, United States

Synopsis
The impaired strength of osteoporotic cortical bone is largely a consequence of increased porosity, which manifests in increased bone water fraction. Hence, knowledge of bone water (BW) content would provide an indirect measure of pore volume fraction. Surface interactions in the tight spaces of the lacuno-canalicular system shorten the lifetime of the BW proton signal to less than 1*m*sec, therefore requiring solid-state imaging techniques for its capture and detection. In this work, we developed new ultra-short echo-time (UTE) radial imaging acquisition and processing capabilities for precise quantification of BW in cortical bone.

Introduction: Cortical bone mechanical competence is a function of both composition and architecture at both the macro-and microstructural level **[1]**. Fracture resistance of cortical bone is adversely affected by an age-related increase cortical porosity **[2]**, which is aggravated in osteoporosis **[1]**. The spaces of the haversian and lacuno-canalicular system making up the total pore volume are fluid-filled, essentially consisting of water. Hence, knowledge of bone water (BW) content would provide an indirect measure of pore volume fraction (even though not all of the detected water is pore water). Since surface interactions of the water confined to the tight spaces of these pores cause the lifetime of the water signal to be extremely short (T_2*<<1*m*sec), solid-state imaging techniques are required for its capture, e.g. **[3]**. Here, we developed new 3D ultra-short echo-time (UTE) radial imaging capabilities for precise quantification of BW concentration (%BWC) which is sensitive to various sources of error, including behavior of gradients affecting the reconstruction of ramp sampled *k*-space, matching of half-sinc paired pulses in two successive acquisitions, 3D coil shading, coherence loss during excitation **[4],** but also to bone water T_1 which increases with increasing pore volume fraction.

Methods:

Data Acquisition: Fig. 1 shows the 3D hybrid radial UTE (3DHRUTE) sequence in conjunction with *selective excitation*; a 5.0cm slab corresponding to a half-pulse with main-lobe duration of about 150μsec and a gradient strength of 2.9*m*T/m to acquire twenty 4.5mm axial slices, centered at 38% of tibia length (site of maximum cortical thickness) measured from medial malleolus. Each slice is obtained using radial readout with ramp sampling on k_x-k_y plane and variable-*TE* on k_z. The minimum RF-to-readout transition time limits *TE* to ~80μsec at k_z=0. Images were acquired at 3T (Siemens Tim Trio, Erlangen, Germany), with FOV=180×180mm^2, 500 radial projections each with 256 readout samples, dwell time = 6μsec ($BW_{\text{read-out}}$ = 650Hz/pixel), TR=20msec and spatial resolution of 0.38×0.38mm^2 in 6.6mins with an 8-channel Tx/Rx knee coil. No soft-tissue suppression was used to avoid systematic errors from partial suppression of the BW signal.

Regridding, reconstruction and gradient mapping: Radial readout with ramp sampling requires regridding which is highly susceptible to small timing errors and non-ideal *k*-space trajectories caused by nonlinearities of readout gradients which are scanner hardware-specific, but not scan object dependent. Thus, we performed gradient mapping calibration by directly measuring the *k*-space trajectory, yielding the effective gradient shape. Once the gradient delays are determined, the timings are adjusted in the reconstruction code as a function of view angles to correct the hardware imperfections prospectively.

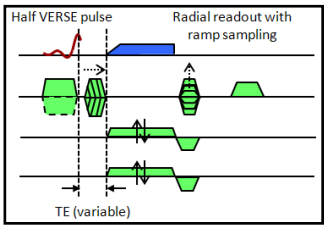

Fig. 1 3D HRUTE utilizing pairs of half-*sinc* pulses, radial readout with ramp sampling and variable-TE on the k_z axis.

Quantification: Eq. 1a expresses BWC, ρ_{bone}, as a function of reference volumetric proton density, ρ_{ref} (20% H_2O in D_2O doped with 27mM $MnCl_2$ yielding T_1~15*m*sec and T_2*~320μsec), bone and the reference signal intensities, I_{bone} and I_{ref}, respectively, factors to account for losses during nutation [**4**], F_{bone} and F_{ref}, effective echo-time, TE_{eff} and effective transverse relaxation rates ($R_2^* \equiv 1/T_2^*$) for bone (T_2*~400μsec) and the reference, R_{2bone}* and R_{2ref}*, respectively. Eq. 1b expresses the relative magnetization as a function of *TR*, T_1, π/T_2^* (τ = RF pulse duration) and pulse shape, in which transverse magnetization is represented by f_{xy} and longitudinal magnetization is represented by f_z **[4]**, and are numerically evaluated for the half-sinc pulse. Such an intensity-based quantification was previously validated *ex-vivo* **[5]**.

$$\rho_{bone} = \rho_{ref}\frac{I_{bone}F_{ref}}{I_{ref}F_{bone}}\exp\left(-TE_{eff}\left(R^*_{2ref}-R^*_{2bone}\right)\right) \quad 1a)$$

$$F = f(T_1,T_2^*,\tau,TR) = f_{xy}\cdot\frac{(1-e^{-TR/T_1})}{(1-f_z\cdot e^{-TR/T_1})} \quad 1b)$$

3D coil shading profile: The 8-channel coil used for the human subject studies consists of an array of 8 surface coils which leads to some inhomogeneity in the received signal. Without correction, this can cause large errors, in particular when bone and reference location substantially differ in coil sensitivity. Here we implemented a simple technique to remove the shading effects based on 3D imaging a large homogenous phantom from which the spatial dependence of the coil sensitivity is derived.

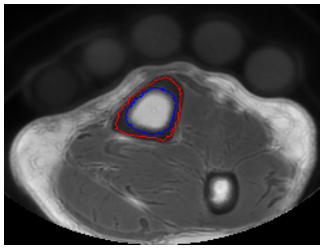

Fig. 2 Coil-shading corrected 3D HRUTE image of tibial mid-shaft with reference samples.

Cortex segmentation for periosteal and endosteal: Segmentation of the cortex from soft tissue is achieved slice by slice using a standard region-growing algorithm to detect the endosteal boundary and a simple intensity-gradient based algorithm to detect the periosteum (Fig. 2).

$$r = \frac{(1-e^{-TR_1/T_1})}{(1-f_z\cdot e^{-TR_1/T_1})}\Big/\frac{(1-e^{-TR_2/T_1})}{(1-f_z\cdot e^{-TR_2/T_1})} \quad 2)$$

T_1-mapping: T_1-maps are generated as follows: 1) a dual-*TR* acquisition is performed in which two radial scans were concatenated with TR_1=20*m*sec and TR_2=60*m*sec, 2) a ratio map, $r(x,y,z)$, is computed by dividing short-*TR* to the long-*TR* intensity images, and 3) $T_1(x,y,z)$, is constructed by solving the non-linear equation expressed in Eq. 2, pixel-by-pixel and for T_1 values (employing inverse optimization methods), assuming nominal values for imaging parameters, e.g. flip-angle, pulse shape, T_{1ref}, T_{2ref}*, T_{2bone}*, etc. Using a flip angle mapping techniques, applied flip angle values are found to be 23˚(nominal)±5%.

Results and Conclusions: Fig. 2 shows an axial image from tibia mid-shaft, after coil shading correction, along with reference samples for bone water quantification. Fig. 3 shows T_1- and BWC images in the center slice (slice #10) for two subjects, with parametric T_1- and BWC-maps superimposed on anatomic images. Longer T_1 is associated with elevated BWC suggesting greater contribution from larger pores to the bone signal in the older subject having more porous bone (larger pores are associated with longer T_1 values as they have lower surface-to-volume ratio). T_1 values associated with pixels in the trabecularized endosteal boundary were excluded from the analysis by setting a threshold at T_1 < 1.5sec. Fig. 4 shows reproducibility data for BWC in 9 healthy subjects, each scanned twice within one month. Intra-class correlation coefficients (ICC) were 0.95 and 0.85 for BWC and T_1, respectively and mean root-mean-square difference for BWC and T_1 of 0.27% and 7.6*m*sec, respectively. There was a weak positive correlation between average T_1 and BWC values (R = 0.35, p = 0.151). In conclusion, our results suggest that cortical bone water concentration can be measured reliably as a means to assess cortical porosity, which is associated with the cortical bone's mechanical competence.

(b)

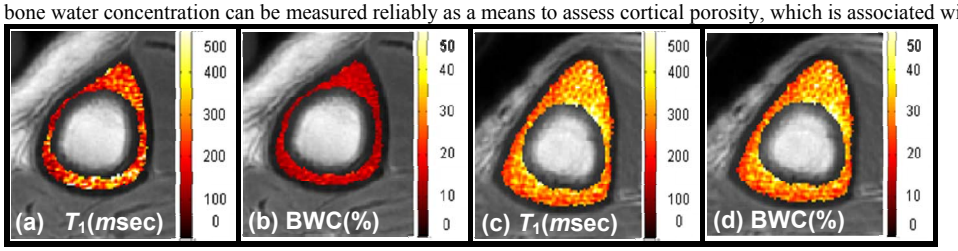

Fig. 3 T_1-map (*m*sec) and BWC-map (%) images for two subjects: (a, b) F, 26 yrs, T_{1avg}=270 *m*sec, BWC=15.1%; (c, d) M 77yrs, T_{1avg}=309 *m*sec, BWC_{avg}=31.0%.

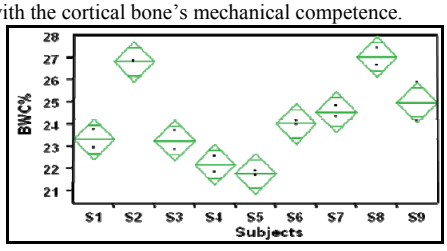

Fig. 4 BWC reproducibility results for 9 healthy subjects at two time points.

References: **[1]** Seeman E *et al.*, *NEJM* 354, 2250 (2006). **[2]** Bousson V *et al*, *JBMR* 19, 794 (2004). **[3]** Robson MD *et al.*, *JCAT* 27, 825 (2003). **[4]** Pauly JM, *et al.*, 28 (1989). **[5]** Techawiboonwong A *et al.*, *Radiology* 248, 824 (2008).

Acknowledgements: ***NIH grant RO1 AR50068***